Langmuir
Article
pubs.acs.org/Langmuir

Microstructure and Rheology of Lime Putty

E. Ruiz-Agudo[†] and C. Rodriguez-Navarro*

Dpto. Mineralogía y Petrología, Facultad de Ciencias, Universidad de Granada, Fuentenueva s/n 18002, Granada, Spain. [†]Present address: Institut für Mineralogie, Universitat Münster, Correnstrass. 24, 48149, Münster, Germany. Telephone: +49 251 8333454. Fax: +49 251 8338397. E-mail: eruiz_01@uni-muenster.de

Received September 11, 2009. Revised Manuscript Received October 28, 2009

The rheology of lime binders, which is critical in the final performance of lime mortars and plasters, is poorly understood, particularly in its relationship with the microstructure and colloidal characteristics of slaked lime ($Ca(OH)_2$) suspensions (i.e., lime putties). Here, the contrasting flow behavior of lime putties obtained upon slaking (hydration) of soft and hard burnt quicklimes (CaO) is compared and discussed in terms of the differences found in particle size, morphology, degree of aggregation, and fractal nature of aggregates as well as their evolution with aging time. We show that lime putties behave as non-Newtonian fluids, with thixotropic and rheopectic behavior observed for hard and soft burnt limes, respectively. Aggregation of portlandite nanoparticles in the aqueous suspension controls the time evolution of the rheological properties of lime putty, which is also influenced by the dominant slaking mechanism, that is, liquid versus vapor slaking in hard and soft burnt quicklimes, respectively. These results may be of relevance in the selection of optimal procedures and conditions for the preparation of lime mortars used in the conservation of historical buildings.

I. Introduction

Slaked (or hydrated) lime, that is, the mineral portlandite ($Ca(OH)_2$), is one of the most common and oldest building materials known to mankind.[1] Over the last two centuries, however, lime has been gradually replaced by hydraulic binders, Portland cement in particular.[2] Nonetheless, the observed incompatibility between Portland-cement-based binders and ancient masonry has resulted in the resurgence of high calcium lime as the binder of choice in mortars and plasters used for the conservation of Architectural Heritage.[1−4] Despite its current use in conservation interventions, knowledge regarding lime binders is mainly based on empirical observations of traditional practice, without a thorough understanding of the scientific basis that rules the performance of lime as a binder in mortars and plasters.[1,3,4] In this respect, one of the main but less understood properties of lime pastes is their rheology.[5]

The first references to the importance of the flow behavior of lime mortars and plasters date back to Vitruvius (30 BC) who praised the excellent plasticity of lime putty.[5] This is the most desirable property of a binder in the fresh state and has a decisive effect on its workability and performance. Despite its importance, studies on the flow behavior of lime putties and pastes, which are known to behave as colloidal suspensions,[6] are scarce. The complex rheology of $Ca(OH)_2$ suspensions and the difficulty in giving a mechanistic interpretation for the observed flow behavior has been recognized.[7,8] Atzeni et al.[5] modeled lime putty as a Bingham fluid, although the low number of data points as well as the low value of the correlation coefficient suggest that the Bingham model may not adequately describe the rheological behavior of lime putty, especially at the low shear rates tested. Latter on, Atzeni et al.[9] studied the rheology of lime putties prepared from limestones with different pore systems and tried to correlate the observed differences in viscosity with the microstructure of the hydroxide, but a study of the particle shape or size distribution was not accomplished. Vávrová and Kotlík[10] compared the rheological properties of fresh and "matured" lime putties prepared from dry hydrate. They pointed out the suitability of viscosity measurements to determine lime putty quality for conservation mortars. In agreement with Atzeni et al.,[5] their measurements indicate that the viscosity of aged putties is higher than that of freshly prepared hydrated lime putties.[10] Again, this latter work lacked an interpretation of the rheological data in terms of the microstructure of the suspension, which ultimately should determine the flow behavior of the putty.

Processing parameters during lime production (i.e., calcination, slaking, and aging) influence the microstructural characteristics of quicklime (CaO) and slaked lime and, in turn, the workability and performance of the lime-based mortar.[1,3,4,11−14] Our preliminary results[15] show that the viscosity of slaked lime putty depends on the microstructure of quicklime, which is mainly

*Corresponding author. Telephone: +34 958 246616. Fax: +34 958 243368. E-mail: carlosrn@ugr.es.

(1) Elert, K.; Rodriguez-Navarro, C.; Sebastian Pardo, E.; Hansen, E.; Cazalla, O. *Stud. Conserv.* **2002**, *47*, 62.
(2) Seabra, M. P.; Labrincha, J. S.; Ferreira, V. M. *J. Eur. Ceram. Soc.* **2007**, *27*, 1735.
(3) Rodriquez-Navarro, C.; Hansen, H.; Ginell, W. S. *J. Am. Ceram. Soc.* **1998**, *81*, 3032.
(4) Hansen, E.; Rodriguez-Navarro, C.; Van Balen, K. *Stud. Conserv.* **2008**, *53*, 9.
(5) Atzeni, C.; Farci, A.; Floris, D.; Meloni, P. *J. Am. Ceram. Soc.* **2004**, *87*, 1764.
(6) Ray, K. W.; Mathers, F. C. *Ind. Eng. Chem.* **1928**, *20*, 475.
(7) Gabard, J. L. *Ciments Betons Platres Chaux* **1997**, *824*, 56.
(8) Sébaïbi, Y.; Dheilly, R. M.; Quéneudec, M. *Construction Building Mater.* **2004**, *18*, 653.
(9) Atzeni, C; Orru, D.; Sanna, U.; Spanu, N. *ZKG Int.* **2006**, *59*, 81.
(10) Vávrová, P.; Kotlík, P. *Meteriály Pro Stavbu* **2003**, *3*, 6.
(11) Boynton, R. S., *Chemistry and Technology of Lime and Limestone* (2nd edition). Wiley, New York, 1981.
(12) Rodriguez-Navarro, C.; Cazalla, O.; Elert, K.; Sebastián, E. *Proc. R. Soc. A* **2002**, *458*, 2261.
(13) Rodriguez-Navarro, C.; Ruiz-Agudo, E.; Ortega-Huertas, M.; Hansen, E. *Langmuir* **2005**, *21*, 10948.
(14) Cazalla, O.; Rodriguez-Navarro, C.; Sebastian, E.; Cultrone, G.; De la Torre, M. J. *J. Am. Ceram. Soc.* **2000**, *83*, 1070.
(15) Ruiz-Agudo E.; Rodriguez-Navarro C. *Libro de Actas del IX Congreso Internacional de Rehabilitación del Patrimonio Arquitectónico y Edificación*, Centro Internacional para la Conservación del Patrimonio, Gran Canaria, **2008**, *1*, 153−158.

determined by limestone calcination conditions that lead to the production of either "soft burnt" or "hard burnt" limes.[11] The slaking of these two products results in completely different lime putty pastes; in the first case, low viscosity and plasticity are observed in the fresh putty, while in the latter a fine paste with a high viscosity is readily obtained. Furthermore, the conditions during CaO slaking (e.g., the water/oxide ratio) and the type of slaking (i.e., vapor versus liquid phase hydration) also appear to influence the lime putty properties, including its rheology. Industrial lime slaking typically involves vapor phase hydration with the stoichiometric amount of water, thus producing a dry hydrate. Conversely, traditional slaking, using excess water, is thought to proceed via liquid phase hydration, resulting in the formation of a slaked lime putty.[11] In general, slaked lime putties show higher plasticity and workability than putties prepared with dry hydrate.[4,9] Furthermore, slaked lime putties typically improve their reactivity, plasticity, and workability following long-term storage under excess water (the so-called "aging").[3−5,10,14] The reason why aging improves the quality of lime putties is still a matter of debate,[16] although it has been suggested that aging results in the formation of submicrometer platelike crystals out of large prismatic portlandite crystals and secondary nucleation of nanometer-sized platelike crystals.[3] Despite the pioneering work by Atzeni et al.,[5] little is currently known on the effects of aging on the rheology of lime putties.

Considering that the physical properties of lime putties are intimately connected with the microstructure of the suspension (i.e., particle size and shape, particle size distribution, and degree of aggregation), it is our aim to study the rheological properties of slaked lime putties and their evolution with aging time, and interpret their flow behavior in terms of the microstructure of the putties. The effect of limestone calcination temperature/retention time (i.e., the microstructure of the quicklime) on the viscosity of the resulting slaked lime paste is also considered. We show that lime putties are non-Newtonian fluids, with a complex behavior that depends on the strain gradient considered. Nanoparticle aggregation controls the time evolution of lime putty viscosity, which also depends on the dominant slaking mechanism, that is, vapor versus liquid phase slaking, occurring in soft and hard burnt quicklimes, respectively. Thixotropic and rheopectic behaviors are also described for the tested lime putties. The results of this work are of particular relevance for the selection of optimal processing parameters to be used in the preparation of lime mortars and plasters for the conservation of cultural heritage.

II. Materials and Methods

II.1. Raw Materials and Preparation of Slaked Lime Putties. Two types of quicklime were used for the preparation of slaked lime putties: a traditionally calcined (hard burnt) quicklime (Francisco Gordillo lime; Seville, Spain; FGQ) and an industrially prepared (soft burnt) quicklime (Andaluza de Cales lime; Seville, Spain; ACQ). Slaked lime putties were prepared in the laboratory by mixing CaO pebbles (ca. 1−2 cm in size) and deionized water under vigorous stirring. The water/oxide weight ratio was 1:4, yielding a slaked lime putty with a typical solid volume fraction, ϕ, of ∼0.24. Values of ϕ ranging from 0.05 up to 0.24 were obtained adding deionized water to the slaked lime putty. The two quicklimes were characterized by means of X-ray diffraction (XRD; Philips PW-1710 diffractometer with an automatic slit; measurement parameters: Cu Kα radiation λ = 1.5405 Å, exploration range from 15° to 35° 2θ, steps of 0.028° 2θ, goniometer speed of 0.01° 2θ s^{-1}), field emission scanning electron microscopy, (FESEM, Leo Gemini 1530), transmission electron microscopy (TEM, Philips CM20, 200 kV acceleration voltage), N_2 sorption (NAD, Micromeritics TriStar 3000), and mercury intrusion porosimetry (MIP, Micromeritics, Autopore 2500). Details on sample preparation and specific characteristics of the above listed analytical equipments have been published elsewhere.[13]

II.2. Reactivity Test. Reactivity tests were performed according to standard ASTM C 110-96a.[17] A total of 250 g of unslaked lime with a particle size of ∼10 mm was added to 1000 g of water at 20 °C in a thermostatically isolated flask. The mixture was continuously stirred at 300 rpm while the temperature rise was monitored with a thermometer and stopwatch.

II.3. Characterization of $Ca(OH)_2$ Particles. To minimize microstructural changes of $Ca(OH)_2$ particles associated with drying, slaked lime putty samples were freeze-dried.[13] Putty samples (with mass ca. 2 g) were collected with a spatula, placed in porcelain cups, and immediately introduced in a Labconco Lyph-Lock 6 freeze-dryer where samples were frozen at −20 °C and sublimated under vacuum (5−10 μmHg) at 25 °C. Afterward, the powdered samples were kept under N_2 atmosphere prior to characterization by means of XRD, FESEM, TEM, MIP, NAD and electrokinetic analyses. Particle size distribution (PSD) of portlandite suspensions was determined both by digital image analysis of TEM photomicrographs (collected at different magnifications) using the Scion Image software and by laser scattering (LS) using a GALAI CIS-1 particle size analyzer. Higher accuracy was found in the case of TEM-PSD for the quantification of submicrometer primary particles, whereas LS-PSD was more discriminating to quantifying larger primary particles and aggregates.[13] The ζ-potential of $Ca(OH)_2$ particles dispersed in saturated $Ca(OH)_2$ aqueous solution (ϕ ∼ 0.01; pH ∼ 12.4) was determined upon electrophoretic meassurements at 25 °C, using a Malvern ZetaSizer 2000 instrument.

II.4. Rheological Measurements. The rheological measurements were carried out on a Brookfield R/S rheometer equipped with coaxial cylinder geometry (inner rotating cylinder (spindle) with a diameter of 12.05 mm, outer stationary cylinder with a diameter of 13.56 mm, and height of 19.6 mm). A constant temperature (T) of 25 (±0.5) °C was maintained during the measurement using a circulatory water bath. Three types of rheological tests were performed: two consisted of the determination of the flow curve of the putties under a controlled shear rate (CR) regime, while the third type of test was performed at a controlled stress (CS) regime in order to determine the yield stress.[18] First, CR tests were done by measuring shear stress (τ, Pa) in three stages: (i) a first stage of logarithmic increase of the shear rate ($\dot{\gamma}$, s^{-1}) from 0 to 1000 s^{-1} in 225 s; (ii) a 30 s plateau at the maximum shear rate (1000 s^{-1}); and (iii) a final step of logarithmic decrease of $\dot{\gamma}$ to 0 s^{-1} in 225 s. Preshearing of the putties (250 s^{-1}, 150 s) was performed in order to avoid the influence of the structure at rest. This first set of rheological tests was performed in freshly prepared slaked lime putties and was intended to precisely characterize the flow behavior of lime putties. In a second set of rheological measurements, the flow curve was determined under CR conditions in three stages: (i) a first stage of linear increase of the shear rate ($\dot{\gamma}$, s^{-1}) from 0 to 250 s^{-1} in 180 s; (ii) a 30 s plateau at the maximum shear rate (250 s^{-1}); and (iii) a final step of linear decrease of $\dot{\gamma}$ to 0 s^{-1} in 180 s. These measurements were aimed at determining the evolution of lime putty rheology upon aging and thus were performed at different periods of time after slaking (up to 3 years aging). The

(16) Thompson, M. In *Proceedings of the International RILEM Workshop on Historic Mortars: Characterization and Tests*; Barton, P., Groot, C., Hughes, J. J., Eds.; RILEM Publications: Paris, 2000; p 163.

(17) ASTM C 1100-96a. *Standard Test Methods for Physical Testing of Quicklime, Hydrated, and Limestone*; American Society for Testing and Materials: Philadelphia, PA, 1997.

(18) Moreno Botella, R. *Reología de suspensiones cerámicas*, Biblioteca de Ciencias, 17. Consejo Superior de Investigaciones Científicas, Madrid, **2005**.

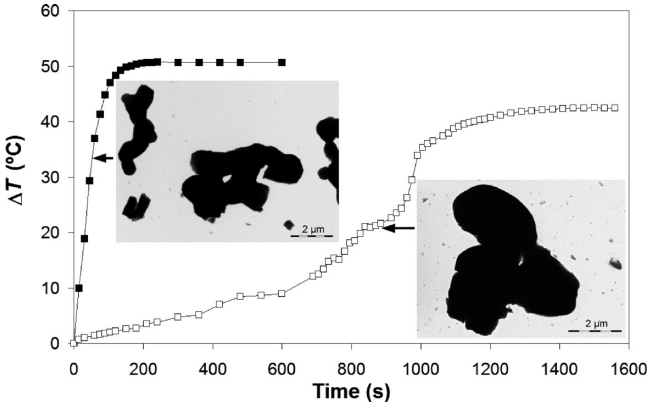

Figure 1. Lime slaking reactivity tests: temperature (T) versus time plots for ACQ (■) and FGQ (□). Representative TEM photomicrographs of the two quicklimes are shown as insets.

viscosity at $\dot{\gamma} = 250\ s^{-1}$ was chosen to monitor the temporal evolution of the rheological behavior of lime putties. Finally, a third set of measurements consisted of the determination of yield stress under a CS regime and at different periods of time after slaking (up to 3 years aging). In these latter tests, shear stress was linearly increased from 0 to 400 Pa in 210 s and the corresponding shear rate was measured.

Due to the highly exothermic nature of the lime slaking process, it was necessary to make the first rheological test 6 h after slaking to ensure that the measurements were made at constant T. Upon completion of the rheological measurements, putty samples were weighed, oven-dried overnight at 110 °C, and reweighed, in order to quantify ϕ (the density, ρ, of $Ca(OH)_2$ is 2.24 g cm^{-3}).[11] Putties were stored in airtight capped containers under excess water throughout the length of testing. To avoid carbonation during storage, flushing with N_2 was performed before airtight capping. Right before testing, excess water was decanted.

III. Results and Discussion

III.1. Microstructure of Quicklimes. XRD analyses showed that both FGQ (hard burnt) and ACQ (soft burnt) quicklimes were highly pure lime (CaO), with trace amounts (< 3 wt %) of calcite ($CaCO_3$). They showed a type-II sorption isotherm (data not shown), typical of essentially nonporous solids.[13] This is consistent with their low surface area. There was, however, a difference of 1 order of magnitude in surface area values of the two quicklimes: that is, 0.5 and 5 $m^2\ g^{-1}$ for FGQ and ACQ, respectively. The micropore volume (N_2 sorption results) was also 1 order of magnitude higher in the case of ACQ (32.5×10^{-5} $cm^3\ g^{-1}$) if compared with FGQ (3.6×10^{-5} $cm^3\ g^{-1}$). A shift in the average pore size (MIP results) toward larger sizes was observed in FGQ (average pore size of 1.06 and 0.27 μm for FGQ and ACQ, respectively). No significant differences in porosity between both quicklimes were detected with MIP ($57 \pm 3\%$ and $55 \pm 3\%$ for ACQ and FGQ, respectively). TEM images show that CaO crystals in ACQ had a smaller particle size and sharper edges than those in FGQ (insets in Figure 1). These results show that the soft burnt ACQ lime underwent limited coarsening via oriented aggregation (as proposed by Rodriguez-Navarro et al.)[19] and sintering, while the hard burnt FGQ lime underwent a higher level of oriented aggregation and sintering of the nascent CaO nanoparticles. The thermal decomposition of the limestone in a traditional kiln involved higher burning temperatures and/or retention time than the industrial calcinations in a rotary kiln,[11] resulting in a hard burnt lime (FGQ) and a soft burnt lime (ACQ), respectively. The smaller particle size of ACQ and its higher surface area made this quicklime more reactive than FGQ. This is confirmed by the faster and higher increase in T observed following slaking of ACQ lime (Figure 1).

(19) Rodriguez-Navarro, C.; Ruiz-Agudo, E; Luque, A; Rodriguez-Navarro, A.; Ortega-Huertas, M. *Am. Mineral.* **2009**, *94*, 578.

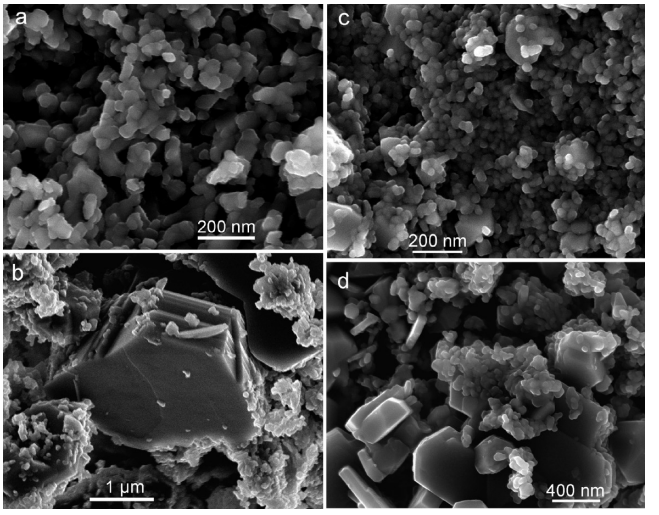

Figure 2. FESEM photomicrographs of (a, b) FGP and (c, d) ACP lime putties. Samples were freeze-dried 6 h after slaking. Aggregates of platelike portlandite nanocrystals (a and c), as well as individual micrometer- (b) and submicrometer-sized (d) prism-shaped crystals are observed.

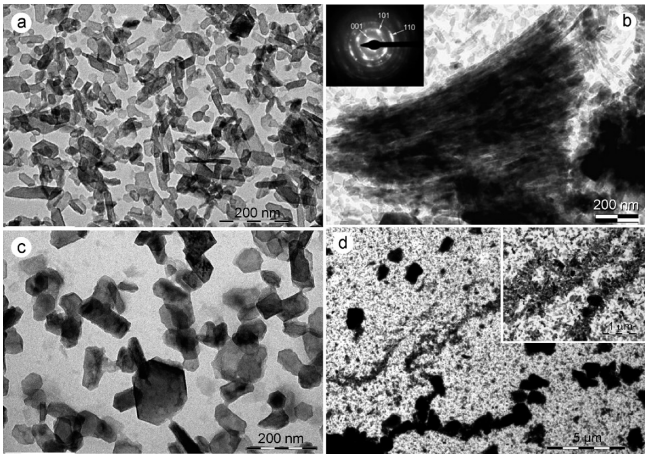

Figure 3. TEM photomicrographs of freeze-dried FGP lime putty. Abundant platelike nanocrystals (a) as well as scarce micrometer-sized oriented aggregates (b) were observed 6 h after slaking. Inset in (b) shows the [010] zone axis SAED pattern of the oriented aggregate with spots corresponding to the 001, 101, and 110 Bragg reflections. Crystals were attached along the (0001) basal planes (which are normal to the image plane). Three years after slaking (aging time), growth of the colloidal crystals (i.e., Ostwald ripening) (c) and formation of large linear aggregates of both nanosized (see detail in inset) and micrometer-sized portlandite crystals (d) were observed.

III.2. Microstructure of Freshly Slaked Lime Putties. Fresh FGP putties (i.e., 6 h after slaking) showed a structure formed by a combination of a few micrometer-sized portlandite prisms (up to ~3 μm in size) and abundant individual hexagonal platelike $Ca(OH)_2$ nanoparticles, ~20 up to ~200 nm in size, according to FESEM images (Figure 2a and b), TEM images (Figure 3a), and TEM-PSD analyses (Figure 4a). Nanoparticles

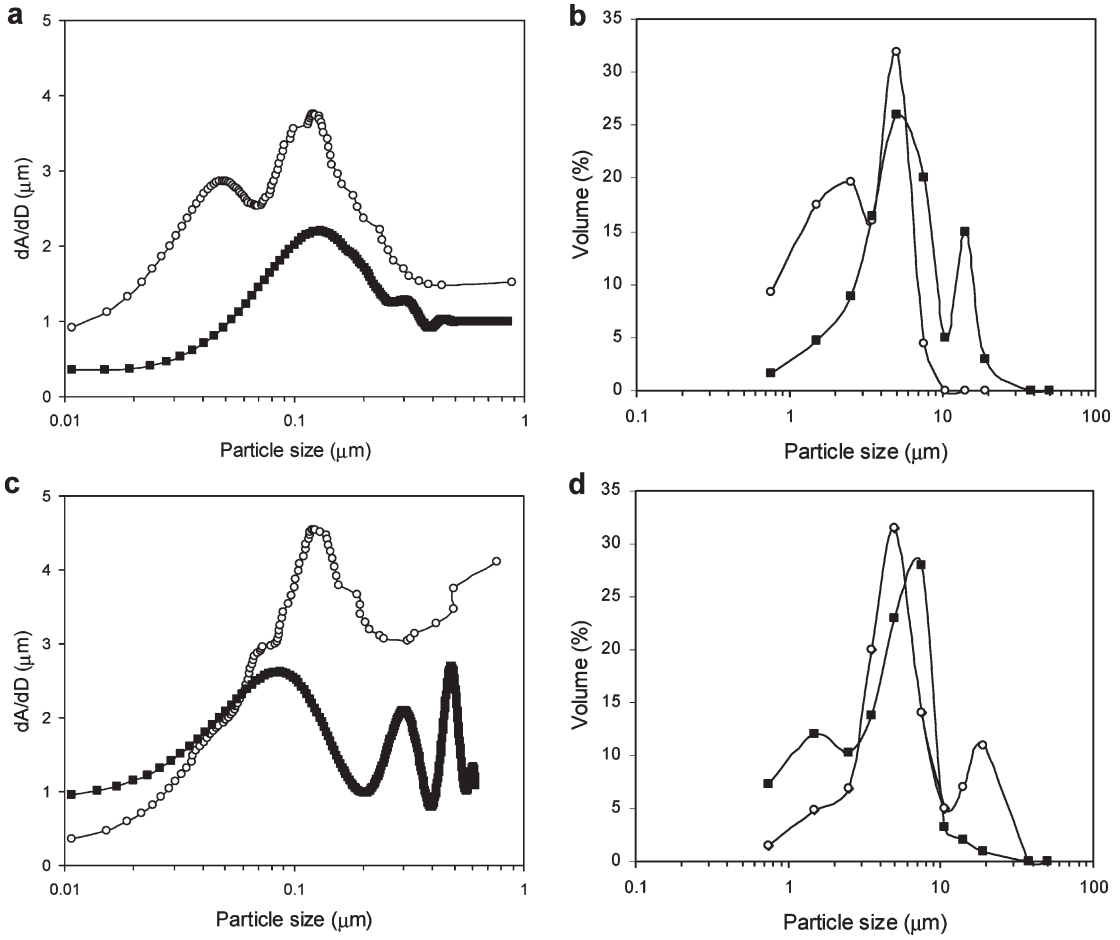

Figure 4. Particle size distribution of FGP (a, b) and ACP (c, d) obtained from digital image analysis of TEM images (a and c) and laser scattering granulometry (b and d). Legend: ○, fresh lime putty (6 h after slaking); ■, aged lime putty (3 years after slaking).

show an average aspect ratio, $r_p = 7.5$ ($r_p = d/l$, where d is the particle length measured along ⟨100⟩ or equivalent ⟨110⟩ and l is its thickness measured along [001]). TEM measurements were used to calculate r_p (average $d = 85$ nm and average $l = 11.5$ nm). Aggregates of platelike portlandite nanocrystals were already observed 6 h after slaking (Figure 3b). Aggregates tended to be larger than the largest individual primary particle. In fact, LS-PSD analyses show a bimodal PSD with a maximum (i.e., mean size) at 5 μm (Figure 4b). Aggregation of primary $Ca(OH)_2$ particles (typically with size $\ll 2$ μm) resulting in secondary particles with mean size of 5−10 μm is a common and thoroughly reported phenomenon.[13,20,21] The peculiarity here is that aggregates in freshly prepared FGP tended to be formed by oriented nanocrystals. Figure 3b shows a detail of a cluster of oriented $Ca(OH)_2$ nanocrystals attached along (0001) planes (i.e., face-to-face aggregation). The corresponding [010] zone axis selected area electron diffraction (SAED) pattern (inset in Figure 3b) confirmed the preferred crystallographic orientation of the nanocrystals in the aggregate. Oriented aggregation of $Ca(OH)_2$ nanocrystals was first reported by Rodriguez-Navarro et al.,[13] who offered a mechanistic explanation for such a phenomenon.

FESEM images of ACP samples (6 h after slaking) (Figure 2c and d) revealed some differences in $Ca(OH)_2$ crystal morphology and size, if compared to FGP particles. Micro- and submicrometer-sized noncolloidal portlandite crystals in ACP were more abundant and showed a higher polydispersity. They also exhibited a preferential development of prismatic faces: that is, they appeared as short $\{10\bar{1}0\}$ prisms caped with {0001} basal pinacoid. TEM analysis of freshly slaked ACP (Figure 5a) revealed that platelike nanocrystals 20 nm up to 60 nm in size were less abundant than in FGP, while colloidal particles with mean size of ∼120 nm were the most abundant (Figure 4c). Colloidal crystals show an average $r_p = 5.9$ (average $d = 120$ nm and average $l = 20$ nm). Nanoparticles in ACP aggregated forming polydisperse round-shaped porous clusters (Figures 4d and 5b), an observation consistent with previous TEM studies of $Ca(OH)_2$.[13] No preferential orientation was observed in these aggregates as shown by the Debye rings in the SAED pattern (inset in Figure 5b). The lower surface area of freshly prepared ACP (if compared with FGP) (Table 1) confirms that a smaller amount of colloidal crystals and a larger number of micrometer-sized portlandite crystals and aggregates were present right after slaking. In fact, LS-PSD analyses showed that the distribution of aggregates was bimodal with mean size at ∼5 μm and ∼20 μm (Figure 4d).

The microstructural differences between the two slaked limes can be explained considering the different microstructure and reactivity of the two quicklimes. According to Wolter et al.,[22] hydration of hard burnt limes (i.e., FGQ) with an excess of water is an interface-advancement (i.e., diffusion-limited) reaction that takes place in the liquid phase. First, a shell of $Ca(OH)_2$ is readily formed surrounding the unreacted CaO core. Afterward, water diffuses through the product layer. The higher molar volume of

(20) Gullett, B. K.; Blom, J. A. *React. Solids* **1987**, *3*, 337.
(21) Arai, Y. *Chemistry of Powder Production*; Chapman & Hall: London, 1996.
(22) Wolter, A.; Luger, S.; Schaefer, G. *ZKG Int.* **2004**, *57*, 60.

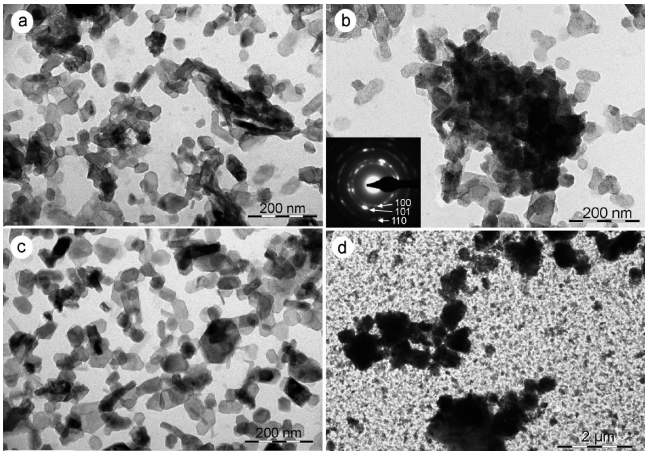

Figure 5. TEM photomicrographs of freeze-dried ACP lime putty: (a) Representative colloidal portlandite crystals 6 h after slaking. (b) Detail of an aggregate present 6 h after slaking and formed essentially by randomly oriented $Ca(OH)_2$ crystals, as shown by the presence of diffraction rings in the SAED pattern (inset). Note however that a few maxima are distinguished which indicate preferential alignment of some of the nanocrystals in the aggregate. (c) Colloidal platelike $Ca(OH)_2$ crystals and (d) heterogeneous aggregates (i.e., formed by large and small crystals) in a 3 year old sample.

Table 1. Effect of Aging on the BET Surface Area of Freeze-Dried Lime Putty Samples

	surface area (m^2 g^{-1})		
	aging time		
sample	6 h	1 month	3 years
FGP	31.7	11.1	7.9
ACP	19.0	20.7	19.8

$Ca(OH)_2$, if compared with CaO, results in cracking and detachment of the product layer. This leads to a significant but delayed increase in the reaction rate, associated with an intense precipitation of colloidal platelike crystals. Such nanosized crystals are similar to those obtained by Arai[21] via homogeneous synthesis under highly supersaturated conditions. Despite the fact that portlandite crystals have a $\zeta = +26 \pm 4$ mV, which means that aggregation should not be favored due to electrostatic repulsion, limited aggregation of primary particles begins right after slaking due to the high ϕ of the suspension.[13] All in all, portlandite particles of a high surface area ($\sim$32 m^2 g^{-1}) are obtained.

In contrast, slaking of soft burnt lime (i.e., ACQ) involves both liquid and (mainly) vapor phase hydration.[22] Because soft burnt quicklimes are highly reactive, the heat of hydration is quickly released, resulting in evaporation of the water trapped within the particles. As a consequence, only water vapor is available within these particles for further reaction, which proceeds at a very fast rate. Beruto et al.[23] have shown that (pure) vapor phase hydration of CaO is a structurally controlled pseudomorphic reaction, leading to a high surface area product, that is, nanosized $Ca(OH)_2$ crystals. We have also observed the formation of abundant nanosized platelike portlandite crystals following (dominantly) vapor phase hydration of ACQ. In our tests, however, massive formation of water vapor bubbles in the bulk of the suspension led to local transient "drying". This in turn should have favored drying-induced aggregation due to the buildup of capillary forces between primary particles,[13,24] resulting in the early formation of the round-shaped clusters observed in freshly slaked ACP. Because an excess of water is available, a final stage takes place (in the case of both soft and hard burnt quicklimes) in which larger portlandite crystals precipitate from the solution at a lower supersaturation. A low supersaturation, which favors growth along the [001] direction,[25] leads to the formation of prismatic portlandite crystals.[21] Overall, a suspension of polydisperse primary particles and abundant micrometer-sized compact aggregates with a lower surface area (ca. 19 m^2 g^{-1}) is produced following slaking of soft burnt ACQ. Such a counterintuitive effect, that is, that a higher reactivity of quicklime leads to a poorer calcium hydroxide (with lower surface area, higher polydispersity, and larger particle size), puzzled researchers for decades[22,26,27] and led to contrasting recommendations regarding which lime (soft or hard burnt) will produce the best hydrate.[11,22] In practice, problems connected to the slaking of highly reactive soft burnt lime can be overcome by adding alcohols to the slaking water. Alcohols and polyols (e.g., diethylene glycol) reduce the slaking rate and maintain the reaction temperature below the boiling point of water, thus preventing or minimizing gas phase hydration. In addition, alcohols lower the surface tension and help preventing agglomeration.[28] The latter effect has been successfully used by Baglioni and co-workers (see Baglioni and Giorgi[29] and references therein) as a means for preparing stable nanosized $Ca(OH)_2$ dispersions that have found a wide range of applications in the conservation of cultural heritage.

III.3. Microstructure of Aged Lime Putties. Aging of FGP led to the growth of primary colloidal particles (Figure 3c) resulting in a significant change in their PSD: from bimodal, with maxima at $\sim$50 and $\sim$120 nm (freshly prepared FGP), to unimodal, with a mean particle size of $\sim$130 nm (3 years aged FGP) (Figure 4a). In addition to the drastic reduction in the amount of the smallest particles, primary particles, both large and small, appeared more aggregated, forming open linear clusters of up to several tenths of crystals as shown by TEM images (Figure 3d). In agreement with TEM observations, LS-PSD analysis of 3 year aged FGP showed the new formation of particles (clusters) 10−20 μm in size (Figure 4b). As a result, the surface area was drastically reduced: nearly to a third (11 m^2 g^{-1}) after 1 month aging and to a fourth (7.9 m^2 g^{-1}) after 3 year aging (Table 1). Figure 4b also shows the disappearance of particles $\sim$2−3 μm in size, mainly corresponding to prism-shaped primary crystals.

Aging of ACP for 3 years led to a reduction in the amount of colloidal crystals with mean size $\sim$120 nm. The remaining colloidal crystals showed a mean size of $\sim$90 nm. Two new classes of submicrometer particles with mean size of 300 and 500 nm appeared (Figure 4c). Apparently, the bigger, rounded clusters found in freshly prepared ACP disaggregated releasing finer particles (Figure 5c). This was confirmed by LS-PSD analyses showing a reduction in the amount of particles with sizes between 10 and 30 μm and 3−7 μm and the increase in the proportion of particles with size $\sim$2 μm and, particularly, < 1 μm (Figure 4d). Nonetheless, a few large (micrometer-sized) crystals and numerous compact aggregates were still present (Figure 5d). Despite the reduction in the amount of larger crystals and aggregates, the

(23) Beruto, D.; Barco, L.; Belleri, G.; Searcy, A. W. *J. Am. Ceram. Soc.* **1981**, *64*, 74.
(24) Scherer, G. W. *J. Am. Ceram. Soc.* **1990**, *73*, 3.
(25) Bhandarkar, S.; Brown, R.; Estrin, J. *J. Cryst. Growth* **1989**, *98*, 843.
(26) Whitman, W.; Davis, G. H. B. *Ind. Eng. Chem.* **1926**, *18*, 118.
(27) Wiersma, D. J.; Hubert, P.; Bolle, J.N. In *Proceedings of the International Lime Association Conference*, Berlin, Germany, **1998**; International Lime Association: Cologne, 1998, 10 p.
(28) Shin, H. G.; Kim, H.; Kim, Y. N.; Lee, H. S. *Curr. Appl. Phys.* **2009**, *9*, S276.
(29) Baglioni, P.; Giorgi, R. *Soft Matter* **2006**, *2*, 293.

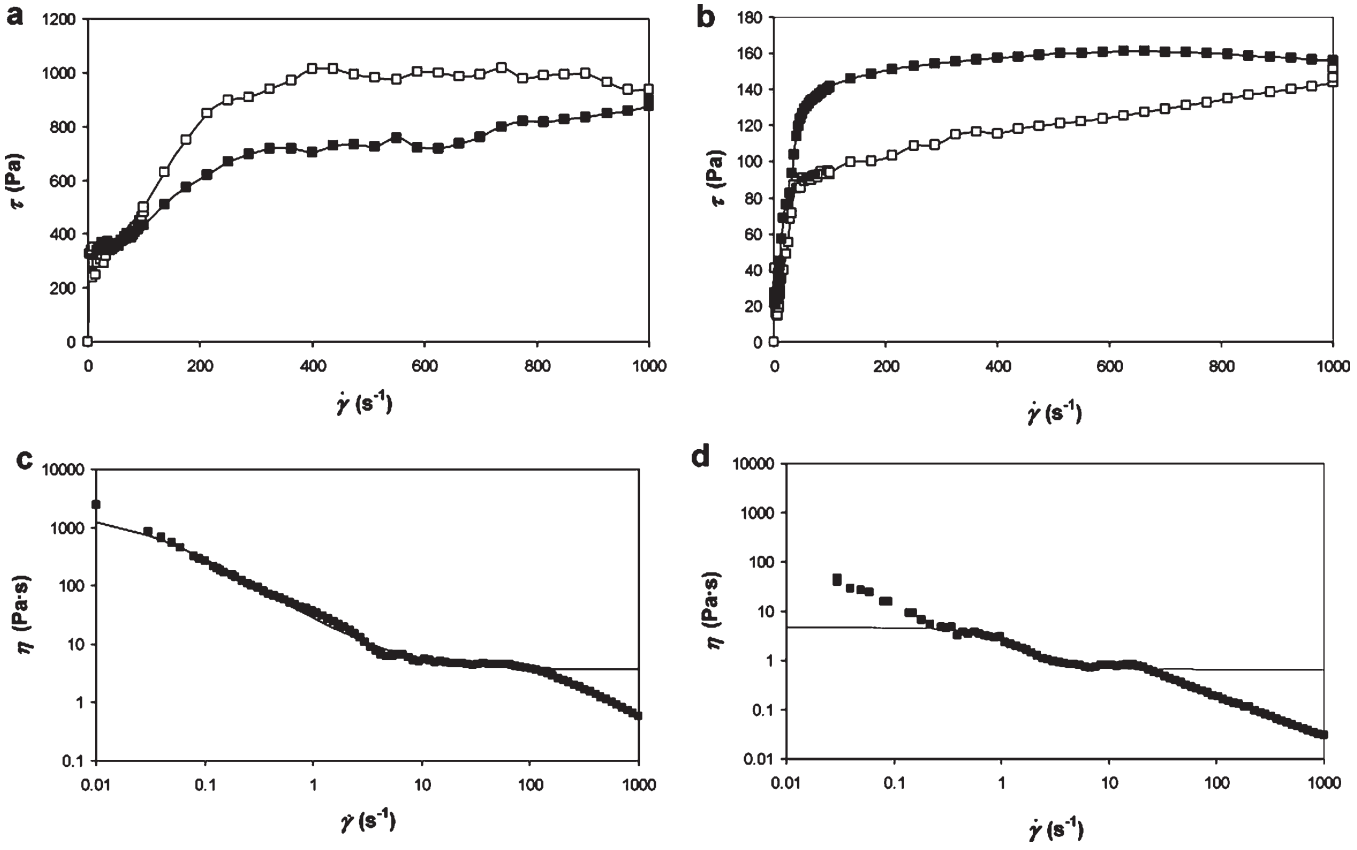

Figure 6. Flow curves for (a) FGP and (b) ACP with a volume fraction of ~0.17 (□, up branch; ■, down branch). Log η versus log $\dot{\gamma}$ plots and fits (solid line) to the Cross model for (c) FGP and (d) ACP. All measurements were performed 6 h after slaking.

surface area of ACP samples remained approximately constant at around 20 $m^2\ g^{-1}$ regardless aging time (Table 1).

Our results show that the type of primary crystals and aggregates formed during and right after lime slaking markedly determine the evolution of the microstructure of the suspension upon aging. Once nucleation occurs, the excess free energy will be compensated by the system by either growth (reduction in the residual supersaturation and Ostwald ripening) or aggregation (decrease in surface energy) of the newly formed crystals.[30] In the case of FGP, the tendency to growth (Ostwald ripening) and aggregation with aging time is expected to be higher compared to ACP. This is due to the smaller size and higher aspect ratio (and, therefore, surface energy) of primary crystals in FGP. Furthermore, face-to-face oriented aggregation of portlandite platelets in FGP seems to be irreversible (at least in the time scale here considered) because the crystallographically controlled bonding among particles forming a cluster is not easily broken.[13] As a consequence, the surface area of FGP is drastically reduced over time, despite the reduction in the amount of micrometer-sized primary prismatic crystals that, as shown by Rodriguez-Navarro et al.,[3] tend to undergo an erosion of their $\{10\bar{1}0\}$ faces, releasing platelike crystals of smaller size as aging progresses.

Besides the initial "drying induced" aggregation, no further massive aggregation is expected in the case of ACP due to the larger size of colloidal particles, higher polydispersity, and abundance of prismatic crystals and, therefore, lower surface energy. Upon aging, the loose, disoriented aggregates formed during slaking of ACQ tend to break. Aging of the larger prismatic crystals can also result in the release of nanometer sized platelike crystals.[3] All in all, finer particles are released which compensate for the growth of the colloidal ones (i.e., Ostwald ripening), keeping the surface area of ACP nearly constant over time.

III.4. Rheological Properties of Fresh Lime Putties. Figure 6 shows representative plots of τ versus $\dot{\gamma}$ and viscosity (η) versus $\dot{\gamma}$ data for freshly prepared FGP and ACP suspensions. The viscosity data demonstrate the complexity of the flow behavior of the lime putties. Typically, colloidal suspensions show a variety of nonlinear rheological properties (yield stress, shear thinning, shear thickening, thixotropy, and/or rheopexy)[31] that depend on interparticle forces, Brownian motion of the particles, and hydrodynamic interactions as well as on the shape, size, and volume fraction of particles, on the degree of aggregation, and on the fraction of fluid immobilized by the particles.[32,33] At low shear rates, a strong shear-thinning behavior, typical of highly concentrated stable colloidal suspensions of ceramic powders,[34] was observed (Figure 6c and d). At higher shear rates, a transition in behavior from non-Newtonian to Newtonian occurred, as shown by the shoulder in the flow curves. This behavior was followed by further shear thinning at higher $\dot{\gamma}$, when hydrodynamic effects were dominant.[33] Modeling of the behavior of the suspensions at both high and low shear rates was done using the Cross model,[35] which is represented by the equation

$$\frac{\eta - \eta_\infty}{\eta_0 - \eta_\infty} = \frac{1}{\left(1 + (K\dot{\gamma})^m\right)} \quad (1)$$

(30) Rodriguez-Clemente, R.; Gomez-Morales, J.; Lopez-Macipe, A.; Garcia-Carmona, J.; Ocaña, M.; Serna, C. J. *Contrib. Sci.* **1999**, *1*, 63–77.

(31) Wessel, R.; Ball, R. C. *Phys. Rev. A* **1992**, *46*, R3008.
(32) Smith, T. L.; Bruce, C. A. *J. Colloid Interface Sci.* **1979**, *72*, 13.
(33) Zaman, A. A.; Dutcher, C. S. *J. Am. Ceram. Soc.* **2006**, *89*, 422.
(34) Bergstrom, L. *Colloids Surf., A* **1998**, *133*, 151.
(35) Cross, M. M. *J. Colloid Sci.* **1965**, *20*, 417.

Table 2. Rheological Parameters of Freshly Slaked Lime Putties

	FGP		ACP	
	low $\dot{\gamma}$	high $\dot{\gamma}$	low $\dot{\gamma}$	high $\dot{\gamma}$
ϕ_{max}[a]	0.24	0.26	0.35	0.35
$[\eta]$[a]	9.09	5.31	15.37	10.98
$[\eta]_0$[b]	7.57	nd	6.28	nd

[a] Calculated by fitting the experimental data to the Krieger−Dougherty equation (eq 2). [b] Determined using eq 3. nd: not determined.

where η_0 and η_∞ are the extrapolation of the viscosity at zero and infinite shear rates, respectively, K is a time constant, and m is a fitting (dimensionless) parameter. Rheological data calculated for different volume fractions were fit to the semiempirical Krieger−Dougherty equation,[36] which for concentrated suspensions gives the dependence of the viscosity with volume fraction as follows:

$$\eta_r = \left(1 - \frac{\phi}{\phi_m}\right)^{-[\eta]\phi_m} \quad (2)$$

where η_r is the relative viscosity ($\eta_r = \eta/\eta_s$) of the suspension, with η_s being the viscosity of the continuum. From these fits, the intrinsic viscosity, $[\eta]$, and the maximum packing fraction, ϕ_m, were determined (Table 2). The intrinsic viscosity of platelike disks and oblate spheroids in the low-shear limit, $[\eta]_0$, is given by the theoretical expression[37]

$$[\eta]_0 = \frac{5}{2} + \frac{32}{15\pi}(r_p - 1) - 0.628\left(\frac{1 - r_p^{-1}}{1 - 0.075 r_p^{-1}}\right), \quad r_p \geq 1 \quad (3)$$

where r_p is the aspect ratio d/l, with d being the diameter of the disk (or oblate spheroid) and l being the particle thickness.

Our experimental and theoretical intrinsic viscosity values (Table 2) are within the range of those reported for suspensions of plate- or disk-shaped colloidal particles. For instance, experimental intrinsic viscosity values of 6.7−10.6 have been reported for suspensions of charge-stabilized colloidal platelike $Al(OH)_3$ particles with aspect ratios very similar to those of the particles described here.[38] Wierenga et al.[39] reported an experimental value of $[\eta] = 23$ for suspensions of gibbsite crystals with an average diameter of 120 nm and a thickness of 13 nm ($r_p = 9.2$). In agreement with the results by Wierenga et al.,[39] our experimental values of $[\eta]$ at the low-shear limit (determined from the fitting of experimental results to eq 2) were higher than those determined using eq 3 (Table 2). Such a discrepancy, which was more evident in the case of ACP suspensions, has been attributed to several factors. Equation 3 is valid for thin disks, and for platelets with $r_p \sim 6$ to 7.5 it is possible that end effects increase the intrinsic viscosity. Similarly, it is plausible that the intrinsic viscosity of hexagonal platelets with sharp vertices is higher than that of smooth disks.[39] Finally, the presence of aggregates also increases the experimental intrinsic viscosity.[32,39] It should be noted that the increase in $[\eta]$ resulting from end effects and particle geometry should be of similar magnitude in both ACP and FGP putties. Therefore, variations in experimental $[\eta]$ must be primarily due to changes in the degree of aggregation. In agreement with the results of the microstructral analysis, the higher experimental $[\eta]$ values of freshly slaked ACP (if compared with FGP) are consistent with its higher degree of aggregation.

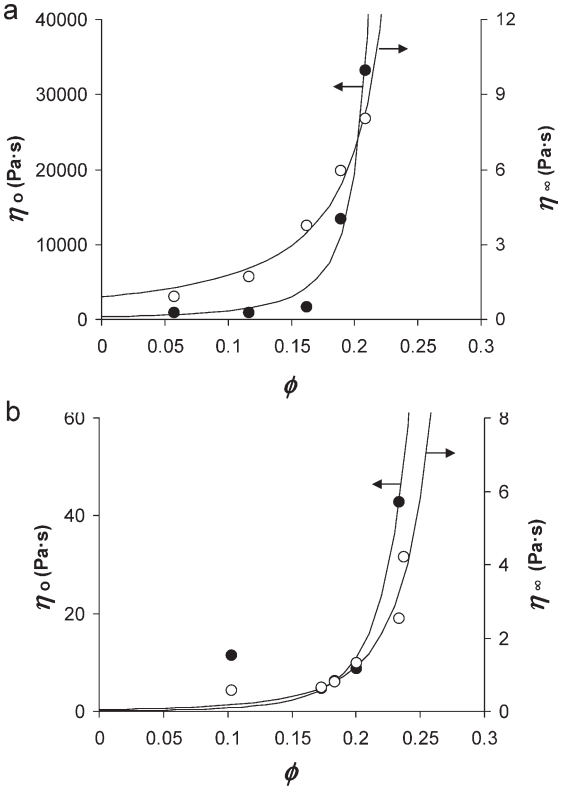

Figure 7. Viscosities at the low, η_0 (●), and high, η_∞ (○), shear limits versus ϕ for (a) FGP and (b) ACP lime putties. η_0 and η_∞ values have been calculated using the Cross model. Solid lines represent the fitting of the Krieger−Dougherty model to the experimental values.

Rheological measurements enable quantification of the fractal nature of a suspension, which helps characterize the type of aggregates formed and the mechanism of aggregation (i.e., diffusion limited or reaction limited) avoiding drying-induced aggregation effects.[13] Evaluation of the flocculated nature of suspensions by means of their fractal dimension can be preformed by correlating the suspension yields stress, σ_0 and ϕ in the form:[40,41]

$$\sigma_0 \approx \phi^m \quad (4)$$

where $m = (d' + X)/(d' - D_f)$, with d' as the Euclidean dimension and D_f and X as the fractal dimensions of the clusters and the backbone of the clusters, respectively. When considering three-dimensional structures, $d' = 3$ and $X \approx 1$ in most of the cases. Fits of yield stress versus volume fraction data to eq 4 are shown in Figure 8. From these fits, the values of fractal dimension were found to be 1.82 ± 0.08 and 2.15 ± 0.20 for FGP and ACP, respectively. The D_f value of FGP is consistent with a diffusion-controlled colloid aggregation mechanism (DLCA, $D_f \sim 1.8$).[42] Such an aggregation mechanism and the resulting fractal dimension are typical of platelet clustering by face-to-face interactions[43] and result in the formation of hard, oriented aggregates such as those observed here. This kind of aggregation has also been

(36) Krieger, I. M.; Dougherty *Trans. Soc. Rheol.* **1959**, *3*, 137.
(37) Kuhn, W.; Kuhn, H. *Helv. Chim. Acta* **1945**, *28*, 97.
(38) Van der Kooij, F. M.; Boek, E. S.; Philipse, A. P. *J. Colloid Interface Sci.* **2001**, *235*, 344.
(39) Wierenga, A. M.; Lenstra, T. A. J.; Philipse, A. P. *Colloids Surf., A* **1998**, *134*, 359.
(40) Shih, W. Y.; Shih, W. H.; Aksay, I. A. *J. Am. Ceram. Soc.* **1999**, *82*, 616.
(41) Tseng, W. J.; Wu, C. H. *Acta Mater.* **2002**, *50*, 3757.
(42) Lin, M. Y.; Lindsay, H. M.; Weitz, D. A.; Ball, R. C.; Klein, R.; Meakin, P. *Nature* **1989**, *339*, 360.
(43) Jin, Z. L.; Hou, W. G.; Li, X. W.; Sun, D. J.; Zhang, C. G. *Chin. Chem. Lett.* **2005**, *16*, 835.

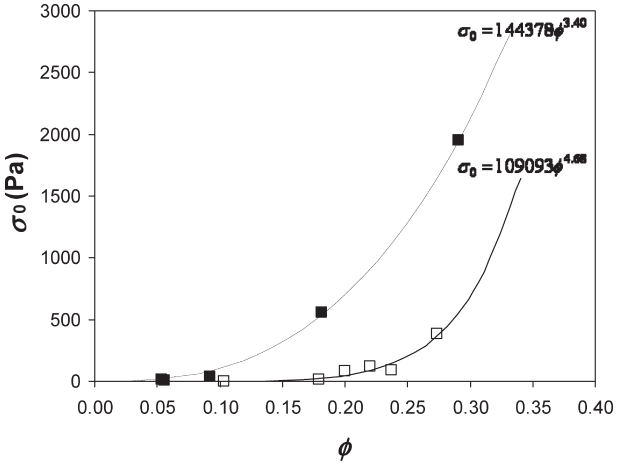

Figure 8. Yield stress (σ_0) versus volume fraction (ϕ) for (■) FGP and (□) ACP. Experimental values are fitted (continuous line) by an exponential function of the type $\sigma_0 = a\phi^m$, where a and m are empirical fitting constants.

visualized by freeze-fracture TEM of concentrated suspensions of magnesium aluminum hydroxide platelike particles.[44] In contrast, the fractal dimension of ACP aggregates is similar to that of reaction controlled colloid aggregation (RLCA, $D_f \sim 2.1$).[42] These aggregates are equidimensional, loose, nonoriented floccules, that most possibly formed massively during local drying associated to the (vapor) slaking process. However, aggregation should also progress after slaking is completed. In this case, it should be noted that if repulsive forces predominate due to the charge of $Ca(OH)_2$ particles, there will be several collisions before sticking leading to a RLCA regimen in both ACP and FGP. However, if collisions occur along the basal planes, which comprise the largest surface of the platelets with a high aspect ratio (i.e., FGP), irreversible attachment due to bonding along these equally oriented planes will be favored. This manifests as oriented attachment and leads to fast aggregation following the DLCA regime.[45]

Any increase in the asymmetry of the particles and/or aggregates should result in an increase in the viscosity (for the same volume fraction). This helps explain why FGP, which includes linear, open aggregates, systematically displays the highest values of viscosity (for equal volume fraction), irrespectively of the shear rate regime considered (Figures 6 and 7). Additionally, the higher amount of platelike nanocrystals in FGP also contributes to a higher viscosity.[5]

In addition to the open, linear aggregates (after face-to-face oriented aggregation) present in FGP, open structures may have formed upon face-to-edge interaction between individual $Ca(OH)_2$ platelets (see comments on thixotropy in the following paragraphs), leading to a high volume of trapped fluid within the aggregates. On the one hand, the presence of these open aggregates results in smaller ϕ_m values than those of ACP (Table 2). On the other hand, because FGP has less free volume available for the particles to move around, so there are more particle−particle interactions, so higher resistance to flow, and hence a higher viscosity.[46]

In contrast, the higher polydispersity of ACP as well as the rounded shape of the aggregates result in higher packing fractions, as the smaller particles (or aggregates) can fill the gaps between coarse crystals (or aggregates).[18] All in all, the viscosity of polydisperse ACP is orders of magnitude smaller than that of equal volume fraction FGP. It is well-known that polydisperse (bimodal or trimodal) colloidal suspensions show lower shear viscosity than that of each individual suspension of monodisperse particles.[33,47,48]

Interestingly, ϕ_m values for both FGP and ACP suspensions are smaller than the theoretical maxima for monodisperse ($\phi_m \sim 0.52-0.74$) and polydisperse ($\phi_m \sim 0.87$) particles.[46] This is partly due to the fact that in our calculations we have not considered the effective volume fraction, ϕ_{eff}, which includes the contribution of the electric double layer. On the other hand, the presence of aggregates with fractal morphology significantly reduces the maximum volume fraction to a limit where the fractal structure of different aggregates begins to interpenetrate. The smaller the value of D_f is, the smaller such a limit is.[49]

One interesting aspect of $Ca(OH)_2$ suspensions that to our knowledge has never been discussed is the pronounced structure formation that takes place during flow. This is reflected by hysteresis loops in the flow curves of both ACP and FGP (Figure 6a, b). In the case of FGP, after a period of shearing at a constant rate (30 s at 1000 s^{-1}), a decrease in viscosity is observed with respect to the viscosity determined from the increasing rate branch of the flow curve (Figure 6a). This phenomenon is known as thixotropy. In contrast, ACP behaves as a rheopectic fluid, that is, that which shows an increase in the viscosity after a period of shearing at a constant shear rate and upon flow cessation (Figure 6b).

The thixotropic characteristics of FGP may be explained by the formation of "card house" structures at rest or at low shear rates due to edge-to-face interactions among free (i.e., nonaggregated) portlandite platelets. At high shear rates, hydrodynamic forces overcome electrostatic interactions and these structures are destroyed. Particles are then aligned with the flow. This is reflected by a decrease in the viscosity of the suspension. In contrast, ACP behaves as a rheopectic fluid. At high shear rates, hydrodynamic stresses can act upon the loose clusters in ACP and fragment them. These stresses are manifested as velocity differences across the structure of the aggregates that produce several fragments of similar size and fluid drag forces that strip primary particles or small floccules from the surface of the original aggregates.[50] As a consequence, both smaller aggregates and individual $Ca(OH)_2$ nanoparticles are released from the original clusters. This causes an increase in the viscosity of the suspension upon relaxation of the flowing system.[51] This behavior may also help to explain the results by Vávrová and Kotlík[10] who indicate that, after prolonged shearing, fresh lime putties showed much higher values of viscosity than nonsheared pastes. A rheopectic behavior has also been reported for suspensions of other structurally equivalent hydroxides such as magnesium aluminum hydroxide.[52]

III.5. Evolution of the Rheology of Lime Putties upon Aging. Substantial differences in the evolution of σ_0 and viscosity at $\dot{\gamma} = 250\ s^{-1}$ (η_{250}) were observed upon aging of ACP and FGP. FGP exhibited a complex rheological behavior that strongly

(44) Albiston, L.; Franklin, K. R.; Lee, E.; Smeulders, J. B. A. F. *J. Mater. Chem.* **1996**, *6*, 871.
(45) Tang, S.; Preece, J. M.; McFarlane, C. M.; Zhang, Z. *J. Colloid Interface Sci.* **2000**, *221*, 114.
(46) Greenwood, R.; Luckham, P. F.; Gregory, T. *J. Colloid Interface Sci.* **1997**, *191*, 11.
(47) Farris, R. J. *Trans. Soc. Rheol.* **1968**, *12*, 281.
(48) D'Haene, P.; Mewis, L. *Rheol. Acta* **1994**, *33*, 165.
(49) Goodwin, J. W.; Hughes, K. W. *Rheology for Chemists: An Introduction*; Royal Society of Chemistry: London, 2000.
(50) Spicer, P. T. Shear-Induced Aggregation-Fragmentation: Mixing and Aggregate Morphology Effects. Ph.D. Dissertation, **1997**.
(51) Butera, R. J.; Wolfe, M. S.; Bender, J.; Wagner, N. J. *Phys. Rev. Lett.* **1996**, *77*, 2117.
(52) Lagaly, G.; Mecking, O.; Penner, D. *Colloid Polym. Sci.* **2001**, *279*, 1090.

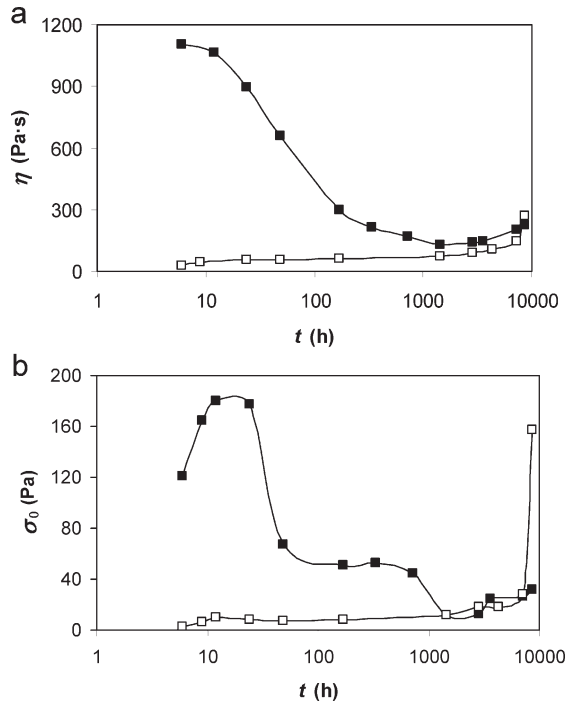

Figure 9. Effect of aging time (t) on the (a) viscosity (η) at constant strain rate $\dot{\gamma} = 250\,s^{-1}$ and (b) yield stress (σ_0) of FGP (■) and ACP (□) lime putties.

depended on aging time (Figure 9). Freshly prepared FGP initially showed a high viscosity, which rapidly decreased, reaching a minimum after a few weeks of aging time. Subsequently, the viscosity tended to increase again after long-term storage (i.e., more than 1 year aging) (Figure 9a). A similar trend was observed in the case of σ_0 versus aging time (Figure 9b). Conversely, the viscosity (Figure 9a) and yield stress (Figure 9b) of soft burnt lime putties (ACP) increased continuously with elapsed time.

Long-term storage of lime putty under water (aging) has been traditionally considered as a way of improving the performance (plasticity, workability, and carbonation kinetics) of lime pastes.[3,4,14,53] However, our results show that this empirical observation is not always that straightforward. Here we have observed that the evolution of the rheological behavior upon aging time depends on the type of quicklime. As it has been already stated, freshly prepared FGP shows a high viscosity due to the massive presence of hexagonal platelike nanoparticles. However, these particles tend to rapidly aggregate into large clusters which markedly increase the mean particle size.[54] This results in a decrease in the viscosity of the putty, which reaches a minimum after a few weeks of storage.[15] These aggregates are hard aggregates that do not easily break by shearing of the suspension. Subsequently, viscosity tends to increase slightly after long-term storage (i.e., more than 1 year). In contrast, viscosity and yield stress of freshly slaked soft burnt lime putties (ACP) are orders of magnitude smaller than those of freshly slaked hard burnt lime putties (FGP). However, the viscosity of ACP tends to increase continuously with aging time. In agreement with Atzeni et al.,[5] aging not only increases the viscosity of lime putty but also results in a significant increase in the yield stress. The smaller amount of platelike nanocrystals in ACP, in addition to its higher ϕ_m (associated to its higher polydispersity), leads to a lower initial viscosity, if compared with FGP. However, the breaking up of the original round-shaped clusters as well as the release of additional submicrometer particles following corrosion of prismatic faces of portlandite crystals undergoing aging are thought to be responsible for such an improvement in the rheological characteristics of ACP as aging progresses. In fact, the (increased amount of) submicrometer particles present in aged ACP have sizes below the critical size $d_c = 620$ nm reported by Zaman and Dutcher[33] for the case of electrostatically stabilized colloidal silica, at which the dependence of viscosity on particle diameter decreases significantly (for $d > d_c$). Hence, an increase of the amount of $Ca(OH)_2$ particles with $d \lesssim 620$ nm with aging time explains the significant increase in the suspension viscosity.

IV. Conclusions

Our rheological study has revealed that lime putties behave as non-Newtonian fluids, with a complex behavior that depends on the strain gradient considered. These results are interpreted in terms of the microstructural characteristics of $Ca(OH)_2$ suspensions.

In the case of the hard burnt lime, the best rheological properties are achieved immediately after slaking, when the nanoparticles are smaller and the micrometer-size platelike crystals are mostly nonaggregated. A high viscosity and, as a consequence, a high plasticity are then obtained, which are the most desired properties for mortar application. Another positive consequence of the initial microstructure of the hard burnt lime putty is that the smaller particle size and higher surface area will make this putty more reactive toward carbonation. These optimal properties worsen quickly with time, although they seem to be partly recovered after long periods of aging. Oriented, face-to-face aggregation of platelike particles via attachment along (0001) planes is thought to be responsible for the observed rapid decrease in surface area, viscosity, and yield stress. This structurally controlled aggregation appears to be irreversible. These results suggest that hard burnt lime putties should be used right after slaking (e.g., for architectural conservation purposes). Otherwise, the initial optimal rheology of the freshly slaked lime putty could be preserved ("frozen") by adding organic compounds (e.g., polyelectrolytes) that upon adsorption on the positively charged surface of the platelike crystals prevent their irreversible aggregation. Studies are currently being performed to explore the effectiveness of such a procedure. Such studies may also aid in the understanding of the positive effects associated to the traditional use of natural organic additives (e.g., plant extracts, ficus or cactus juice, casein, just to name a few) in lime slaking.[55]

In the case of slaked lime putties prepared with a soft burnt quicklime, the initial structure of the suspension is formed mainly by noncolloidal prismatic portlandite crystals and aggregates of randomly oriented nanometer-sized $Ca(OH)_2$ particles, with a relatively smaller amount of nonaggregated colloidal platelike portlandite crystals. Early randomly oriented aggregation, which is associated to vapor slaking (i.e., drying-induced aggregation following water vapor bubble formation in the bulk of the suspension), seems to be reversible. Aggregates break during prolonged storage under water, releasing smaller aggregates as well as single nanosized portlandite crystals. Corrosion of prismatic faces in portlandite micrometer-sized crystals, leading to the

(53) Abell, A. B.; Nichols, J. M. *ASTM Spec. Tech. Publ.* **2002**, *1432*, 23.
(54) Hedin, R. *Plasticity of lime mortars*; National Lime Association: Washington, DC, 1963.
(55) Cowper, A. D. *Lime and Lime Mortars*; Building Research Establishment: London, 1927.

release of submicrometer-sized platelike crystals, also occurred upon aging. These two effects may explain the continuous amelioration of the rheological properties of this putty upon long-term storage under water.

All in all, this work represents one of the few existing rationale studies of the (macroscopic) rheological properties of lime putty in terms of its microstructure and may represent a useful source of information for conservators in the process of selection of the appropriate materials and procedures for the formulation and preparation of conservation mortars.

Acknowledgment. This work has been financially supported by the Spanish government under Contract MAT2006-00578 and the Junta de Andalucía Research Group RNM-179. FESEM, TEM, and PSD analyses were performed at the Centro de Instrumentación Científica of the Universidad de Granada. We thank A. Luque for her help in the acquisition of the two quicklimes (samples were donated by F. Gordillo S.L. and Andaluza de Cales, S.A.). We also thank M. Almecija for her assistance during freeze-drying and R. Hendrickx for helpful comments.